A *Mycobacterium tuberculosis*-Derived Lipid Inhibits Membrane Fusion by Modulating Lipid Membrane Domains

Eri Hayakawa,*† Fuyuki Tokumasu,† Glenn A. Nardone,‡ Albert J. Jin,§ Vince A. Hackley,¶ and James A. Dvorak†

*Precursory Research for Embryonic Science and Technology, Japan Science and Technology Agency, 4-1-8, Honcho, Kawaguchi, Saitama, 332-0012, Japan; †Laboratory of Malaria and Vector Research, National Institute of Allergy and Infectious Diseases; ‡Research Technology Branch, National Institute of Allergy and Infectious Diseases; and §Division of Bioengineering and Physical Science, ORS/OD, National Institutes of Health, Bethesda, Maryland 20892-5766; and ¶Materials Science and Engineering Laboratory, National Institute of Standards and Technology, Gaithersburg, Maryland 20899-8520

ABSTRACT Tuberculosis is an infectious and potentially fatal disease caused by the acid-fast bacillus *Mycobacterium tuberculosis* (MTB). One hallmark of a tuberculosis infection is the ability of the bacterium to subvert the normal macrophage defense mechanism of the host immune response. Lipoarabinomannan (LAM), an integral component of the MTB cell wall, is released when MTBs are taken into phagosomes and has been reported to be involved in the inhibition of phago-lysosomal (P-L) fusion. However, the physical chemistry of the effects of LAM on lipid membrane structure relative to P-L fusion has not been studied. We produced membranes in vitro composed of dioleoylphosphatidylcholine, sphingomyelin, and cholesterol to simulate phagosomal lipid membranes and quantified the effects of the addition of LAM to these membranes, using fluorescence resonance energy transfer assays and atomic force microscopy. We found that LAM inhibits vesicle fusion and markedly alters lipid membrane domain morphology and sphingomyelin-chollesterol/dioleoylphosphatidylcholine ratios. These data demonstrate that LAM induces a dramatic reorganization of lipid membranes in vitro and clarifies the role of LAM in the inhibition of P-L fusion and the survival of the MTB within the macrophage.

INTRODUCTION

Tuberculosis, one of the major maladies afflicting humankind (1–3), is an infectious disease caused by *Mycobacterium tuberculosis* (MTB). The disease afflicts ~1/3 of the human race with over 8 million people becoming infected every year and ≈2 million people dying from the disease (4). Drugs such as antibiotics can be used to treat tuberculosis, but MTB can rapidly develop multidrug resistance (5). Upon entry into the body, MTB bacilli are engulfed by macrophages into phagosomes which would normally fuse with lysosomes and destroy the invading organism. However, live MTB bacilli inhibit phago-lysosomal (P-L) fusion, which subverts this critical initial phase of the macrophage defense mechanism. Consequently, MTB escape the normal acidification process that occurs within the phagosome, permitting them to survive and reproduce.

In addition to peptidoglycans, glycolipids, protein, and lipids, MTBs also contain two unique cell wall lipids (6), a lipoarabinomannan (LAM), and a sulfolipid (7,8). It has been proposed (9–11) that LAM, a 17-kD molecular mass lipoglycan with mannan and arabinan groups and a multiglycosylated extension of a phosphatidylinositol mannoside (12) may be involved in the inhibition of P-L fusion. Specifically, the mannose cap portion of LAM is considered to be essential for the inhibition of P-L fusion (13). Although LAM inhibits increases in cytosolic Ca^{2+}, which induces phagosome maturation (14) and activates phosphatidylinositol 3-kinase (15) which inhibits apoptosis, there are no data concerning the possible role of LAM on membrane properties and the P-L fusion process. A similar situation exists with respect to the MTB sulfolipid (16). However, no major differences in either pathogenicity or growth have been found between sulfolipid-deficient MTB mutants and wild-type MTB (17) implying that the sulfolipid does not play a role in the inhibition of P-L fusion.

Human alveolar macrophage phagosomal membranes are derived from and have a lipid composition similar to plasma membranes, i.e., ≈31% (w/w) phosphatidylcholine (PC), ≈21% (w/w) phosphatidylethanolamine (PE), ≈6.6% (w/w) sphingomyelin (SM), and ≈7.9% (w/w) cholesterol (chol) (18). Chol plays a major role in mycobacterial host cell interactions; MTB cannot invade chol-deficient macrophages in vitro (19). However, if phagosomes are chol depleted in vitro with methyl-β-cyclodextrin, an aspartate-containing MTB coat protein (tryptophane aspartate-containing coat protein, TACO) promotes MTB-phagosome association and P-L fusion (19,20). These phenomena imply that the presence or absence of chol can markedly influence P-L fusion. Therefore, the presence of LAM and its recruitment into chol-depleted lipid microdomains may be sufficient to change the overall membrane domain structure, resulting in an inhibition of P-L fusion. Here we present the results of a multiparametric study of the effects of LAM on lipid domain formation using phagosome-mimicking

Submitted January 9, 2007, and accepted for publication August 3, 2007.

James A. Dvorak passed away on February 5, 2007.

Address reprint requests to Fuyuki Tokumasu, Laboratory of Malaria and Vector Research, National Institute of Allergy and Infectious Diseases, National Institutes of Health, Room 2W-09B Twinbrook III, 12735 Twinbrook Parkway, Bethesda, MD 20892-8132. Tel.: 301-451-1224; Fax: 301-480-1438; E-mail: ftokumasu@niaid.nih.gov.

Editor: Akihiro Kusumi.

0006-3495/07/12/4018/13 $2.00

doi: 10.1529/biophysj.107.104075

membranes produced in vitro to elucidate a possible mechanism whereby LAM inhibits lipid vesicle fusion.

MATERIALS AND METHODS

Materials

1,2-Dioleoyl-*sn*-glycerol-3-phosphocholine (DOPC), 1,2-dioleoyl-*sn*-glycero-3-phosphoethanolamine (DOPE), SM (chicken egg derived), chol, and 1,2-dipalmitoyl-*sn*-glycero-3-phosphoethanolamine-*N*- (Lissamine Rhodamine B Sulfonyl) (N-Rh-PE) were purchased from Avanti Polar Lipids (Alabaster, AL). LAM (Lot M3N9754) was purchased from NACALAI TE SQUE (Kyoto, Japan). V-1 grade muscovite mica (Lot 1090115) was purchased from Structure Probe (West Chester, PA). *N*-(7-nitrobenz-2-oxa-1,3-diazol-4-yl)- 1,2-dihexadecanoyl-*sn*-glycero-3-phosphoethanol-amine, triethylammonium salt (N-NBD-PE) was purchased from Invitrogen (Carlsbad, CA). Reagent grade chloroform and methanol were purchased from Mallinckrodt Baker (Phillipsburg, NJ). Polyethylene glycol 8000 (PEG 8000) was purchased from Fisher Scientific Company (Pittsburgh, PA).

Liposome preparation

The DOPC/SM ratio was adjusted to 1:1 (mol/mol %) and the chol concentration was adjusted to 30 mol % of DOPC+SM in a 3:1 chloroform/methanol solution. The total lipid concentration (DOPC+SM+chol) for fluorescence resonance energy transfer (FRET) was 0.52 mM, and for atomic force microscopy (AFM) measurements it was 1 mg/ml. The LAM concentration was adjusted to 1.8% (w/w) of the three-lipid mixture based on the biochemical data of the tuberculosis cell wall (21): we estimated that LAM concentration is ≈1.57% to 3.74% for total lipids of tuberculosis. The solvent was removed using a stream of Ar gas, and the lipid mixture was dried overnight in a vacuum desiccator ($\approx 10^{-2}$ torr). The dried lipid films were hydrated in Tris-Cl buffer (pH 7.4) at 50°C for 1 h and converted to multilamellar vesicles by vortexing. Large unilamellar vesicles (LUVs) were prepared by 21 extrusion cycles with an Avanti Polar Lipid extruder at 50°C using a 0.1-μm pore size polycarbonate membrane (Whatman, Florham Park, NJ). The protocol used to prepare samples for FRET assays was the same as used to prepare dynamic light scattering (DLS) and AFM samples except that 0.5 mol % of the fluorescent probes N-NBD-PE and N-Rh-PE were incorporated into one of the vesicle samples.

Thin-layer chromatography sample preparation

A 500 μL sample of LAM-containing vesicles prepared as described above was placed in the upper chamber of a Nanosep Omega spin filter tube with a molecular mass cutoff of 300 kDa (35-nm pore size, nominal biomolecular size 90–200 nm) (Cat No. OD300C33; Pall, Ann Arbor, MI). The sample was centrifuged at 4000 rpm for 20 min based on the results of control experiments (see Results) followed by three washes of the filter with 500 μL of a 50 mM NaCl solution. The four samples from the lower chamber below the filter were stored in separate vials for analyses; the first sample was labeled as BOTTOM. Finally, the upper chamber above the filter was rinsed once again with 500 μL of a 50 mM NaCl solution, collected, pooled, and labeled as TOP.

Methods

TLC analyses

A LAM standard in the range of 0.5–1 μg was applied to thin-layer chromatography (TLC) plates (silica gel 60, 5 × 10 cm; EMD Chemicals, Gibbstown, NJ). The plates were developed in chloroform/methanol 0.22% (w/v) $CaCl_2$ (aq) at 65:35:8 (vol). LAM was visualized by spraying the plates with a solution of 0.2% orcinol (Sigma, St. Louis, MO) in 4 N sulfuric acid (Sigma) and heating at 110°C. The lipids were visualized by spraying with a solution containing 10% copper sulfate (w/v) (Sigma) and 10% phosphoric acid (w/v) (Sigma) followed by charring at 120°C.

Dynamic light scattering measurements

Determinations of lipid vesicle size were performed by DLS at 25°C ± 0.1°C using a Malvern Zetasizer 3000HS photon correlation spectrometer with a 256-channel Malvern 7132 correlator (Malvern Instruments, Southborough, MA). The instrument uses a 5 mW He-Ne laser source at 632.8 nm and a fixed scattering angle of 90°. LAM (−) and LAM (+) lipid vesicle samples were prepared as described above and diluted to 1.25 × 10^{-2} mg/ml with a prefiltered, particle-free 50 mM NaCl solution. The samples were sealed in standard glass cuvettes for analysis. Dilution and sample transfer were performed on a Class 100 laminar-flow clean bench. A minimum of 10 measurements of each sample were averaged to generate mean size distributions. Automatic instrument settings were used to select the measurement duration for a determination of the photon autocorrelation function, $g^2(\tau)$. Analyses of the measured correlation functions yielded the diffusion coefficients of the scatterers (22), which, assuming a spherical geometry, were converted to particle sizes using the Stokes-Einstein relation $D = kT/3\pi\eta d_H$, where D is the translational diffusion coefficient of the scatterer, k is Boltzmann's constant, T is the absolute temperature, η is the viscosity of the medium, and d_H is the hydrodynamic diameter of the particle.

We used two methods of analysis to extract size information from the measured correlation functions. The method of cumulants (23) was used to calculate the z-average hydrodynamic diameter and the polydispersity index (PI). The latter describes the width of the z-average distribution. The method of cumulants is the basis for the determination of the average DLS diameter as defined by international standard (ISO 13321: particle size analysis-photon correlation spectroscopy). A second method, using a nonnegatively constrained least squares (NNLS) deconvolution algorithm (23) supplied with the instrument, was employed to generate intensity-weighted particle distributions.

The resulting distributions were fitted with a lognormal function using Origin ver. 7.5J (Origin Lab, Northampton, MA) to obtain the modal diameter.

Fluorescence resonance energy transfer assays

We prepared two vesicle samples. One of the samples contained two fluorescent probes (N-NBD-PE and N-Rh-PE); the other sample was probe-free. Vesicle fusion was monitored by FRET between the donor (N-NBD-PE) and the receptor (N-Rh-PE) molecules (24). All fluorescence measurements were made using a fluorescence spectrophotometer (F-4500, Tokyo, Hitachi, Japan). PEG 8000 was used as a fusion-inducing agent to obtain a maximum fusion rate (25). Sample temperature was maintained at 26°C with a temperature-controlled, circulating water bath. The fluorescent probes were excited at 480 nm, and emission intensity was detected at 580 nm. Data were plotted and analyzed using Origin 7.5J.

Atomic force microscopy

Supported membrane bilayers, both LAM (−) and LAM (+), were prepared on mica by spontaneous vesicle fusion at either room temperature or ≈50°C for 3–10 min as described previously (26). Images were obtained by liquid-tapping mode AFM at a scan rate of ≈1.5 Hz using a multimode AFM, a type D scanner, a Nanoscope IIIa controller, and silicon nitride DNP-S probes with a nominal spring constant of 0.58 N/m (Digital Instruments, Veeco Metrology, Santa Barbara, CA). AFM was performed at 5°C, 26°C, or 37°C in a custom-built, temperature-controlled environmental chamber (modified Model EC02; Sun Electronic Systems, Titusville, FL). The AFM images were stored in a 512 × 512 pixel format and converted to an 8-bit

linear gray scale tagged image file format for image analyses. Domain size and height analyses were performed using Image Pro Plus, version 4.5 (Media Cybernetics, Silver Spring, MD). The perimeter and area data for each domain were analyzed using a multipeak Gaussian window model and statistical analyses of numeric data were carried out using Origin 7.5J. All size measurements were corrected for the effect of AFM probe tip broadening (27).

RESULTS

Incorporation of LAM in DOPC-SM-chol vesicle

LAM contains polysaccharide making it hydrophilic and less soluble in organic solvents. Consequently, since we used a conventional method to prepare vesicles that involved organic solvents to mix the lipid components, it was necessary to verify the incorporation of LAM into the vesicle bilayer. In a control TLC study a 50 mM NaCl solution of free LAM was spin-filtered at three centrifugal speeds (i.e., 3000, 3500, and 4000 rpm) using a 300 kDa filter. LAM passed through the filter at all three speeds (Fig. 1 *A*, BOTTOM). However, at 3000 rpm, a small portion of the LAM remained above the filter in the TOP portion; below 3000 rpm a large portion of the LAM solution remained in the top compartment (data not shown). TLC analyses using standards demonstrated that the LAM remained at the origin on the plate probably due to its large size, degree of glycolysation, and strong hydrophilicity.

SM, DOPC, and Chol were visualized in both the TOP and BOTTOM fractions on the copper sulfate-treated charred plate (Fig. 1 *B*), demonstrating that some vesicles passed through the filter (Fig. 1 *B*, left 2 lanes). However, lower amounts of SM, DOPC, and Chol were detected in the BOTTOM sample of LAM-containing vesicles than the corresponding TOP sample, implying that a larger number of LAM-containing vesicles were retained above the filter than passed through it (Fig. 1 *B*, right 2 lanes). This indicates that the incorporation of LAM into lipid vesicles either increased vesicle membrane rigidity and effective size or modified their surface chemistry, resulting in a stronger interaction with the filter which impeded their passage. In contrast, the orcinol-mediated LAM visualization method demonstrated that free LAM can pass through the filter even though control vesicles coexist in the suspension (Fig. 1 *C*, left 2 lanes). In the LAM-containing sample, a darker LAM spot in the TOP compartment was detected compared to the BOTTOM compartment (Fig. 1 *C*, right 2 lanes). Since free LAM molecules can pass through the filter but LAM-containing vesicles cannot under these conditions, these data demonstrate that LAM can be successfully incorporated on or into lipid vesicles using a conventional LUV preparation method.

DLS characterization of the effects of LAM on vesicles

We used DLS to determine the three-dimensional hydrodynamic sizes of LAM (−) and LAM (+) LUVs. DLS characterizes the surface topography of an object based on a *z*-average of the vesicle diameters. We found that the *z*-average vesicle diameter of LAM (−) LUVs was 133.4 ± 1.1 nm (mean ± SE) and of LAM (+) LUVs was 143.8 ± 1.6 nm. The data were well described as lognormal distributions (Fig. 2). The peak values of these distributions

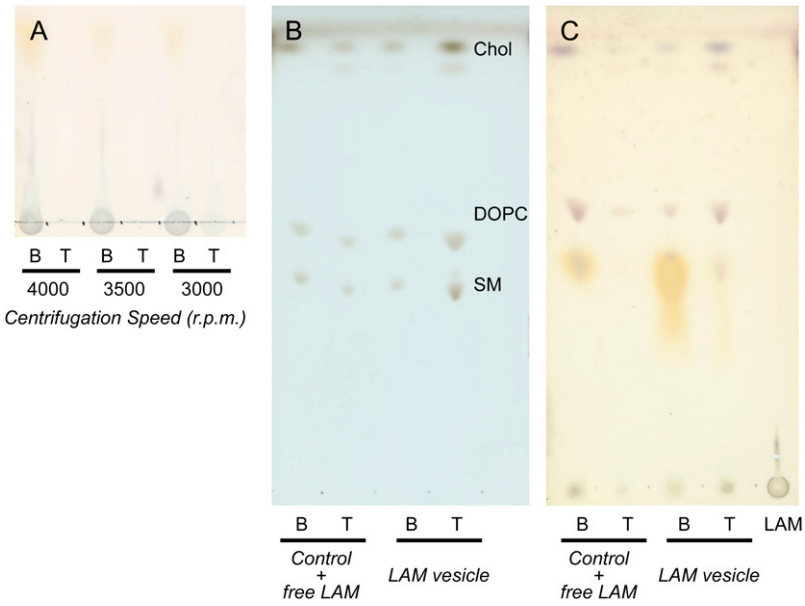

FIGURE 1 TLC analyses on the effects of centrifugal force and filter pore size on the incorporation of LAM into lipid vesicle membranes using spin filtration with a 300 kDa cutoff filter. (*A*) The majority of free LAM passed through the filter. LAM appeared in the BOTTOM fraction at 3500 rpm or higher. However, a small portion of the LAM remained in the top compartment. The yellow spot present in the BOTTOM fraction (*top* of plate) is glycerol, a ''wetting'' agent present in the spin filter which reacts with Orcinol. (*B*) Vesicles can migrate through the filter at 4000 rpm. Although they were present in both the BOTTOM and TOP fractions, a higher proportion of LAM-containing vesicles remained in the TOP compartment of the filter. The faint spot below the chol spot (*top*, LAM vesicle fraction) probably represents oxidized chol derivatives. (*C*) Using the same sample preparation conditions presented in *B*, free LAM in the ''control+LAM'' sample appeared in the BOTTOM filter compartment. In the LAM-containing sample, a higher concentration of LAM was present in the TOP filter compartment. A weaker LAM spot in the BOTTOM filter compartment represents LAM in ''filtered'' vesicles. A free LAM standard is shown on the right. The TLC plate was developed with a chloroform/methanol 0.22% (w/v) $CaCl_2$(aq) at 65:35:8 (vol) solvent system, and LAM was visualized using a 0.2% orcinol in 4 N sulfuric acid solution followed by heating at 110°C. B, BOTTOM; T, TOP; ''control'', LAM-free vesicles.

for LAM (−) and LAM (+) vesicles were 137.9 ± 0.9 nm and 150.7 ± 0.9 nm, respectively. The difference in diameters may identify a portion of LAM molecule protruding out of the vesicle. We used a spherical-shell model of LAM molecules and vesicles to evaluate the size differences between LAM (−)- and LAM (+)-containing vesicles (APPENDIX A). The model is based on the assumption that a symmetric distribution of LAM between the outside and inside leaflets of the lipid membrane resulted in a diameter of 138 nm for LAM (−) vesicles and 151 nm for LAM (+) vesicles (APPENDIX B). These values are indistinguishable from the values obtained by DLS. Therefore, we concluded that LAM molecules are incorporated into the lipid bilayer and the water-soluble sugar moiety of the LAM molecule is exposed to the aqueous environment.

FRET characterization of the effects of LAM on vesicles

It has been reported that MTB releases LAM within a phagosome where it is subsequently transported to the cytosol and plasma membrane (11) and inhibits phagosome maturation, allowing MTB to avoid the lethally low pH of an antibacterial environment. This was the motivation to conduct a FRET study of the effect of LAM on vesicle fusion. In the absence of LAM, rhodamine fluorescence intensity increased along with the PEG concentration change (5–15 wt %), but few fusions occurred at 5% of PEG (Fig. 3 *A*). In contrast, fluorescence intensities of LAM-containing samples were lower than those at equivalent PEG concentrations in the LAM-free system (Fig. 3 *B*). When the PEG concentration was increased to 15 wt %, a much higher fusion rate was seen in the LAM (+) sample, demonstrating that high levels of PEG can overcame the inhibitory effects of LAM. In both LAM (−) and LAM (+), increasing PEG concentration resulted in higher fluorescence fluctuations. However, an addition of LAM suppressed the level of fluctuations in all PEG concentrations as compared to LAM (−) samples. In addition, fluorescence intensities in LAM (+) reached plateau much earlier than in LAM (−) at all PEG concentrations.

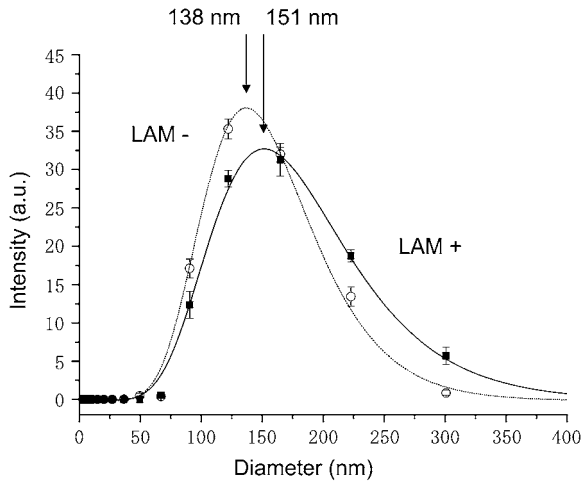

FIGURE 2 DLS assay demonstrates that LAM modulates vesicle diameter size. In the absence of LAM (*dotted line*), the peak value occurred at 138 nm; in the presence of LAM (*solid line*), the peak value shifted to 151 nm.

Fig. 3 *C* shows that the comparison of FRET signals intensities at 10 wt % PEG. In the absence of LAM, the rhodamine fluorescence intensity increased by 12% and reached a plateau in ≈50 min. However, in the presence of LAM the fluorescence intensity increased only ≈2% (plateau reached at ≈12–13 min). From Fig. 3, *A–C*, LAM clearly demonstrates inhibition of PEG-induced vesicle adhesion or fusion or both.

AFM characterization of the effects of LAM on DOPC-SM domains

Giocondi et al. (28) demonstrated the occurrence of the phase separation between DOPC and SM by AFM. Our AFM analyses demonstrated that phase separations in similar domain structures also could be influenced by the addition of LAM. In the absence of LAM, a phase separation between DOPC and SM (Fig. 4 *A*) occurred as a consequence of the difference in the phase transition temperature of the individual lipid components in the mixture. The height difference between the two phases was ≈0.98 nm. However, in the presence of LAM, the size of SM domains increased whereas the total area occupied by the SM domains decreased ≈70% (Fig. 4 *B*). Fig. 4, *C* and *D*, shows enlarged views of Fig. 4, *A* and *B*, respectively, and Fig. 4, *E* and *F*, shows the cross sections of domains in Fig. 4, *C* and *D*, respectively. There is no apparent difference of domain height at 26°C between LAM (−) and LAM (+). The domains were stable at this temperature for at least several hours, and their morphology did not change as a result of repeated scanning (data not shown).

With LAM (+) DOPC-SM samples, we observed membrane structures ranging in size from ≈9.5 to ≈120 nm, and the height range was ≈2–7.7 nm. Structures with ≈120 nm width probably represent aggregates resulting from unfused vesicles. A heterogeneous group of structures with an overall mean population size ranging 17–40 nm probably contains LAM and are similar to previously described supramolecular structures produced by self-assembly (29). Structures in the ≈9.5 nm range probably represent monomers, dimers, or small polymers of LAM. Considering the fact that a single bilayer is ≈5 nm thick (26), the height data suggest that these dots include both LAM self-assembled polymers and that compressed and/or deformed vesicles occurred during the membrane fusion process leading to a supported planer membrane (30). There would be a value slightly lower (≈7.7 nm) than double membrane (5 nm + 5 nm) as a consequence of compression of unfused vesicles by AFM probe.

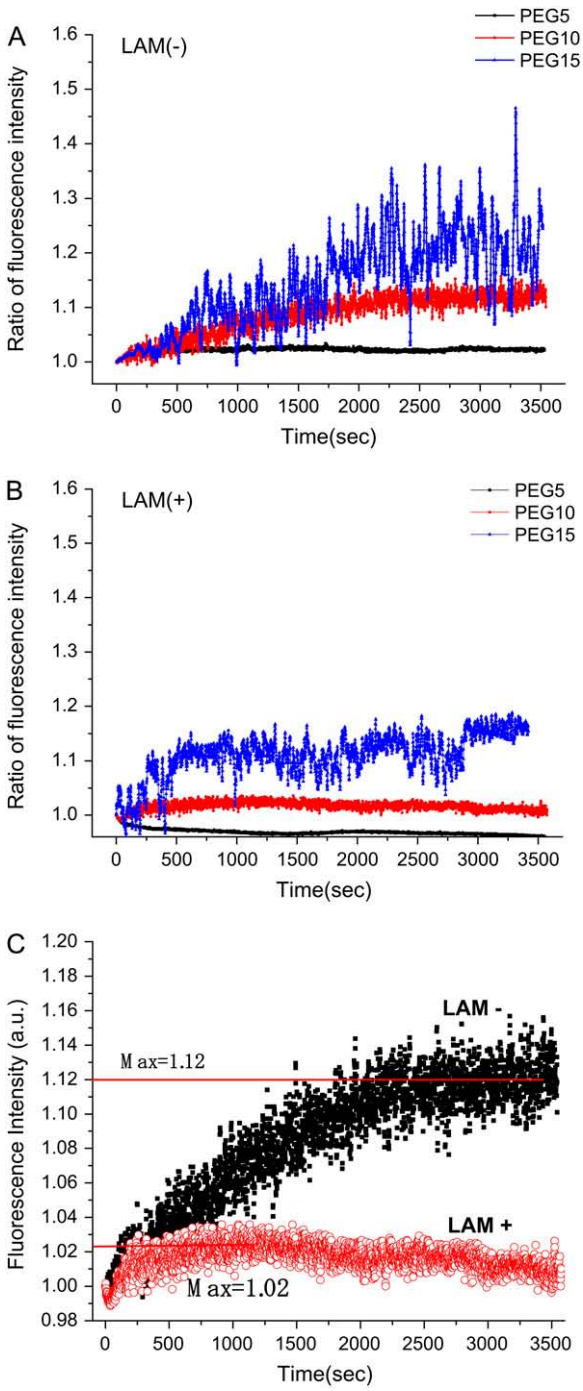

FIGURE 3 FRET assays of the fluorescence intensity profiles of (*A*) LAM (−) and LAM (+) (*B*) vesicles demonstrate that LAM inhibits PEG-induced vesicle fusion. Changes in fluorescence intensity with respect to PEG concentrations (5, 10, 15 wt %) are shown. Fluorescence intensity was slightly decreased at 5% PEG in LAM (+) (*B*), due to possible vesicle aggregations occurring locally. (*C*) A comparison of fluorescence intensity with and without LAM at 10 wt % PEG. In the case of LAM (−) vesicles, the fluorescence intensity increased continuously and reached a plateau at ≈50 min. However, in LAM (+) vesicles there was only a slight change in fluorescence intensity.

It is reasonable to presume that the inositol portion of LAM is in the chol-rich fraction of the domain, and self-assembled LAM polymers are present in domains containing DOPC and SM, although we could not detect by AFM either individual LAM headgroups or their location, possibly due to the compression of long LAM headgroups by AFM probes. Our AFM data support and extend our FRET data, demonstrating that the presence of LAM modulates topographic properties of the membrane, increases phase separations, and inhibits vesicle fusion.

AFM characterization of the effects of LAM on Chol-containing DOPC-SM domains

Chol is an important constituent of macrophage membranes (18) and modulates MTB invasion (19). It has been shown by AFM that SM-chol domains are taller than DOPC domains (31). These height differences allowed us to quantify the effects of the addition of chol on DOPC-SM domain structures. The membrane height difference between LAM (−) and LAM (+) was 0.63 ± 0.20 nm (Fig. 5 *E*) and 0.64 ± 0.08 nm (Fig. 5 *F*), respectively. The presence of chol in SM-chol domains should result in a change in domain structure. However, the total area occupied by SM domains with or without chol was essentially the same (Figs. 4 *A* and 5 *A*). In contrast, when LAM was included in the DOPC-SM-chol mixture, the SM-chol domain size decreased and the domain peripheries become very irregular (Fig. 5 *B*), implying that the inclusion of LAM also modulates and disrupts SM-chol domains.

Temperature also modulated the topographic properties of the membrane domains. At 5°C, in the absence of LAM (Fig. 6 *A*) the SM-chol domains were continuous and occupied a major portion of the membrane surface; at 26°C (Fig. 6 *B*) and 37°C (Fig. 6 *C*), the SM-chol domains decreased in size by 35% and 70%, respectively. However, in the presence of LAM, the SM-chol domains also occupied a major portion of the membrane at 5°C (Fig. 6 *D*) and again became smaller at 26°C (Fig. 6 *E*). The majority of these domains were interconnected and instead of simply decreasing in size, they became fragmented. This phenomenon was even more evident at 37°C where the domains took on a lace-like appearance (Fig. 6 *F*). Table 1 shows the effect of temperature on domain height in LAM (−) and LAM (+). Both in LAM (−) and LAM (+) samples, SM-chol domain height decreased with an increase of temperature. At 5°C, domain height in LAM (+) was higher than that in LAM (−). However, at 26°C and 37°C, domain heights are essentially indistinguishable between LAM (−) and LAM (+). Therefore, the decrease in domain height of LAM (+) from 5°C to 26°C was more than twofold that of LAM (−).

The relationships between temperature and the surface coverage of the SM-chol/DOPC domain with or without LAM are shown in Fig. 7 *A*. The surface coverage by SM-chol domains in LAM (+) is larger than LAM (−) at each

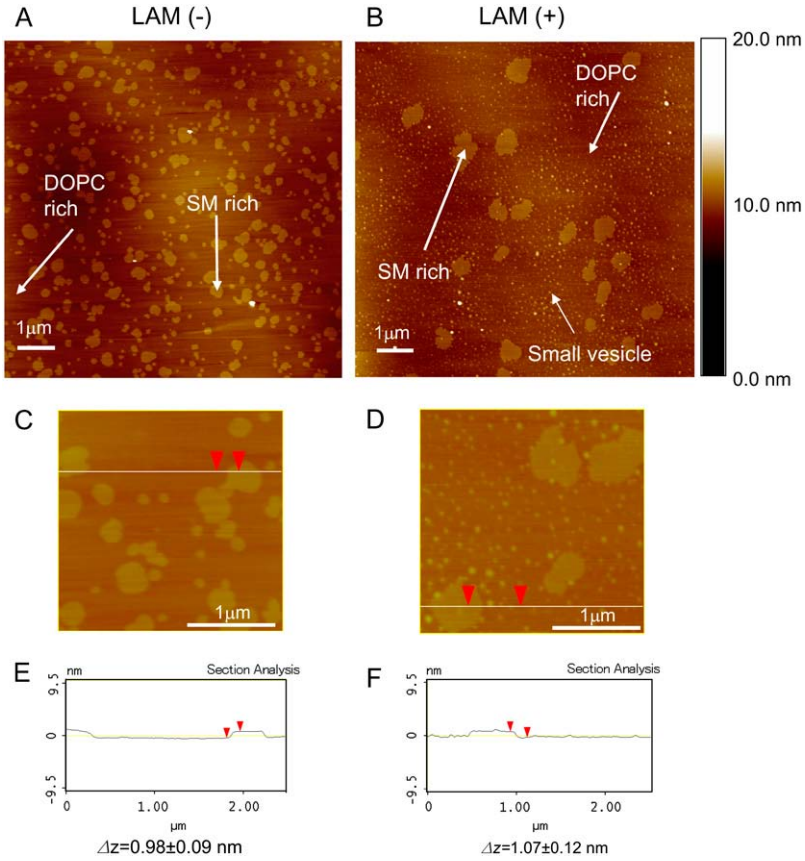

FIGURE 4 In contrast to the exclusion of LAM (−) (*A*), the inclusion of LAM (+) (*B*) into DOPC-SM-chol membrane vesicles resulted in the appearance of larger domains as well as an increased number of small unfused vesicles. *C* and *D* are enlarged views of *A* and *B*, respectively. *E* and *F* show cross sections of SM-chol domains, respectively. A multipeak Gaussian fitting analysis was used to obtain domain height based on optical density differences of the image.

temperature, especially at 37°C: the difference of the surface coverage is more than 20%. To illustrate the dynamic change of domain surface coverage with temperature change, we also plotted ratios between SM-chol and DOPC domains with respect to temperature (Fig. 7 *B*). In the absence of LAM, the SM-chol/DOPC domain ratio decreased linearly as a function of temperature. In contrast, in the presence of LAM the domain ratio decreased exponentially. These results demonstrate that LAM prevents the phase separation process and alters SM-chol/DOPC domain ratios over a physiological temperature range even though changes in domain shape occurred.

Fig. 8, *A* and *B*, shows the length and area of each SM-chol domain in LAM (−) and LAM (+) samples. Although some domains in LAM (+) showed higher length and area, the majority of domains had similar length and area values (Fig. 8, *B* and *C*). Therefore, we used the concept which evaluates the complexity of domain shape (Fig. 8 *C*) on a one-to-one basis. When object shape becomes more complex than the circle while keeping the same area, the perimeter of the object increases beyond $2\pi r$, where r is the radius of the original circle. Therefore, the difference between the domain perimeter and $2\pi r$ can be a measure of the level of complexity of domain shape. Based on this concept, we analyzed the area/length histogram by multipeak Gaussian fitting: two peaks appeared both in the presence and absence of LAM (Fig. 8, *D* and *E*). In the absence of LAM, the peaks occurred at 7.7 ± 1.4 (nm^{-1}) and 12.9 ± 0.9 (nm^{-1}) (Fig. 8 *D*). In the presence of LAM, the peaks occurred at 12.8 ± 0.5 (nm^{-1}) and 21.4 ± 0.7 (nm^{-1}) (Fig. 8 *E*). Table 2 summarizes the perimeter/area population ratios with or without LAM at three different temperatures. At 5°C, the positions of the LAM (−) and LAM (+) peaks were statistically indistinguishable. At 26°C, although the LAM (+) peaks shifted to higher values than at 5°C, there was still no significant different between the 5°C and 26°C values of the LAM (−) peaks. However, at 37°C, the LAM (+) peak values were significantly higher than LAM (−) peak values, confirming the observation that LAM (+) membrane domain irregularities dramatically increased. These data demonstrate that LAM directly affects the phase behavior of the lipid bilayer, more specifically, domain formation or phase separation, probably by modulating intermolecular interactions between the lipid species.

DISCUSSION

LAM in cytoplasm membrane

LAM is known to be released from MTB into phagosome and transported to cytoplasm via phagosomal membrane (2). Furthermore, Shabaana et al. reported that soluble LAM is

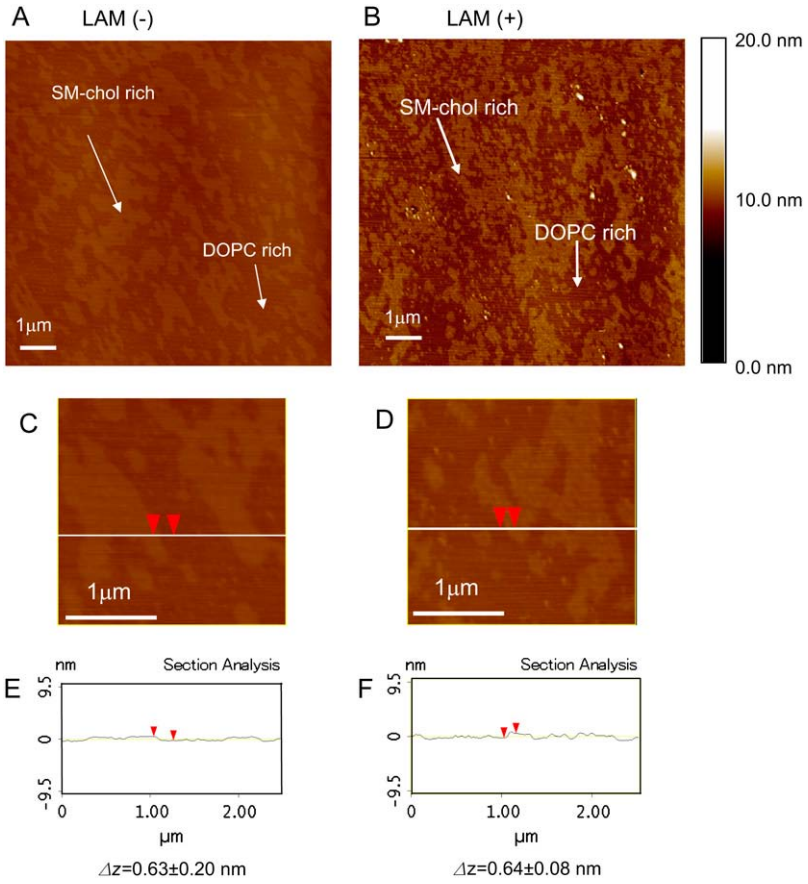

FIGURE 5 The absence (*A*) or presence (*B*) of LAM from lipid membranes resulted in clear changes in lipid domain size and morphology at 26°C. In the absence of LAM, the addition of chol resulted in an increase in domain size. However, when LAM was added to a DOPC-SM-chol membrane, the SM-chol domains decreased in size and their periphery became markedly irregular. *C* and *D* are enlarged views of *A* and *B*, respectively. *E* and *F* show the cross sections of SM-chol domains. A multipeak Gaussian fitting analysis was used to obtain domain height based on optical density differences of the image.

passively incorporated into the raft domain of vesicle membrane (32). When living MTB is captured into phagosome, the phagosomal-lysosomal fusion does not occur. Taken together, LAM may spontaneously insert into the phagosomal membrane, including its outer leaflet, of the infected macrophage and modulate the lipid membrane properties and fusion process.

Two steps of inhibition of membrane fusion by LAM

We focused on the effects of LAM on lipid domain structure and its relation to the inhibition of P-L fusion and demonstrated that LAM inhibits PEG-induced lipid vesicle fusion with FRET in vitro (Fig. 3 and Supplementary Material). An increase in fluorescence intensity provides direct proof that vesicle fusions occurred in the presence of PEG. In our FRET system, the fluorescence probe N-Rh-PE acts as an acceptor and emits light as a consequence of energy transfer from the N-NBD-PE donor probe. If vesicle aggregation and/or lysis occurs between probe (+)-vesicles and probe (−)-vesicles, N-Rh-PE-induced fluorescence intensity would not occur.

In general, the membrane fusion mechanism can be divided into two steps: the first step is vesicle adhesion and the second step is actual vesicle fusion process. The function of PEG in this system is to absorb water molecules around the lipid vesicles and promote membrane associations. In Fig. 3, we demonstrated that LAM inhibits PEG-induced vesicle fusion. Moreover, not only is absolute intensity lower with LAM, but the time required for reaching plateau is also significantly shorter in the presence of LAM compared to LAM (−). These data suggest multiple effects by LAM on fusion process. In fact, another lipid system with PE, which is known as a fusion promoter due to its molecular structure (33), also showed inhibition by LAM (Supplemental Material and Fig. 3) with a different FRET signal pattern. Fluorescence intensities smoothly increased with time in both LAM (+) and LAM (−) with PE. However, the fluorescence intensities are inhibited strongly by LAM in the presence of PE. These data may demonstrate that LAM modulates not only vesicle adhesion but also the after membrane fusion process.

The first step: inhibition of vesicle association

Lower FRET signals with LAM and its enhancement by increase in PEG concentration (Fig. 3) show that LAM effectively reduces the association level of adjacent vesicles. The inhibition of vesicle association in the presence of LAM

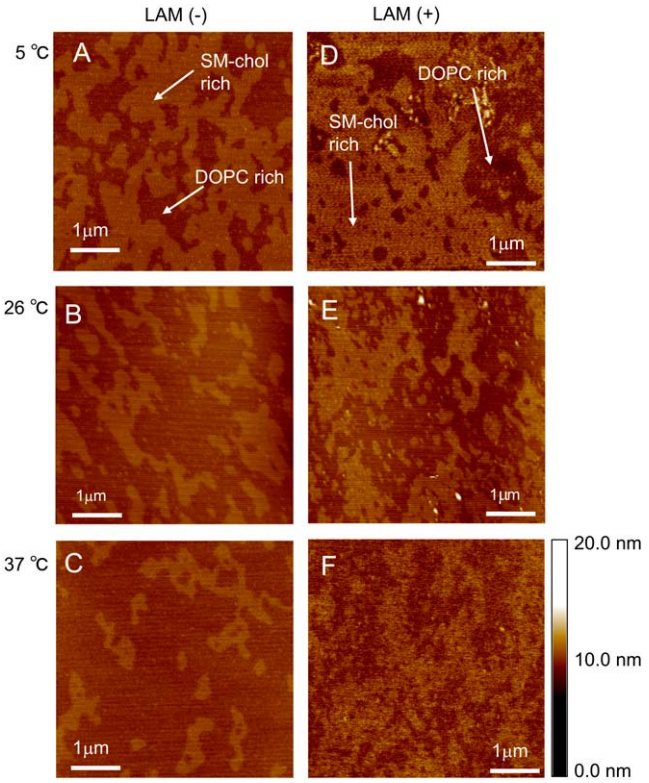

FIGURE 6 The presence of LAM (*D–F*) promoted marked SM-chol domain shape changes over a wide temperature range. In a LAM-free system (*A–C*), SM-chol domain size decreased with increasing temperature. However, the SM-chol domains in a LAM (+) system are highly fragmented and their shapes became more complex.

could be a consequence of either the inability of PEG to extract water molecules from LAM-containing lipid vesicles and/or an obstruction of vesicle fusion by the long sugar chains present in the LAM molecules. Detailed mechanisms of the LAM-induced reductions in vesicle association remains to be studied, but the P-L fusion may also be inhibited on association step with a similar mechanism when LAM is inserted into the phagosomal membrane.

TABLE 1 The effect of temperature on domain height with and without LAM

Temp	LAM (−) (nm)	Δ	LAM (+) (nm)	Δ
5°C	0.67 ± 0.04	−7%	0.76 ± 0.17	−15%
26°C	0.63 ± 0.20	−21%	0.64 ± 0.08	−19%
37°C	0.50 ± 0.07		0.52 ± 0.13	

The height data were obtained by multipeak Gaussian fitting of histograms constructed based on the optical diffuse contrast of captured AFM images. Multiple locations over several images were analyzed to obtain statistical data for each height value. SM-chol domain height became lower by increasing temperature with and without LAM samples. SM-chol domain height is slightly higher in LAM (+) than LAM (−) at 5°C, and it is indistinguishable at 26°C and 37°C.

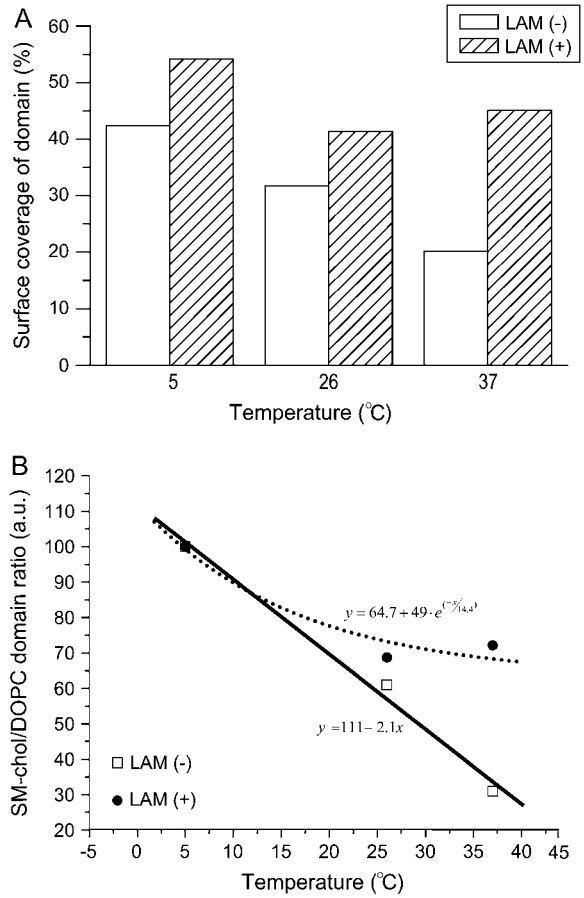

FIGURE 7 (*A*) Surface domain (SM-chol) area of LAM (−) and LAM (+) at three different temperatures. At all temperatures, the SM-chol domain area of LAM (+) is larger than that of LAM (−). The inclusion of LAM (*solid line*) altered DOPC-SM-chol and SM-chol domain ratios over a large temperature range (*B*). However, at physiological temperatures, LAM stabilized SM-chol ratios (*dotted line*).

Second fusion step and LAM-induced modulation of lipid packing

Our AFM data showed that under the same conditions used in the FRET experiments, LAM dramatically changes the SM-chol domain size, height, and structure. In addition, the existence of scattered domains and a nonlinear relationship between temperature and the SM-chol/DOPC domain ratio in LAM-containing membranes (Fig. 7 *B*) are also relevant and provide notable observations substantiating our model of the effects of LAM on lipid membranes. These results increase the possibility that LAM sugar moieties may shield the dipole moments involved in the interactions between phospholipids molecules and change the lipid packing array (34), leading to marked differences in lipid phase behavior at physiological temperature. As a result, lipid domain formation and its shape are altered. Furthermore, the coalescence of small SM-chol domains to form larger domains as well as the maintenance of lipid-packing conditions in each domain

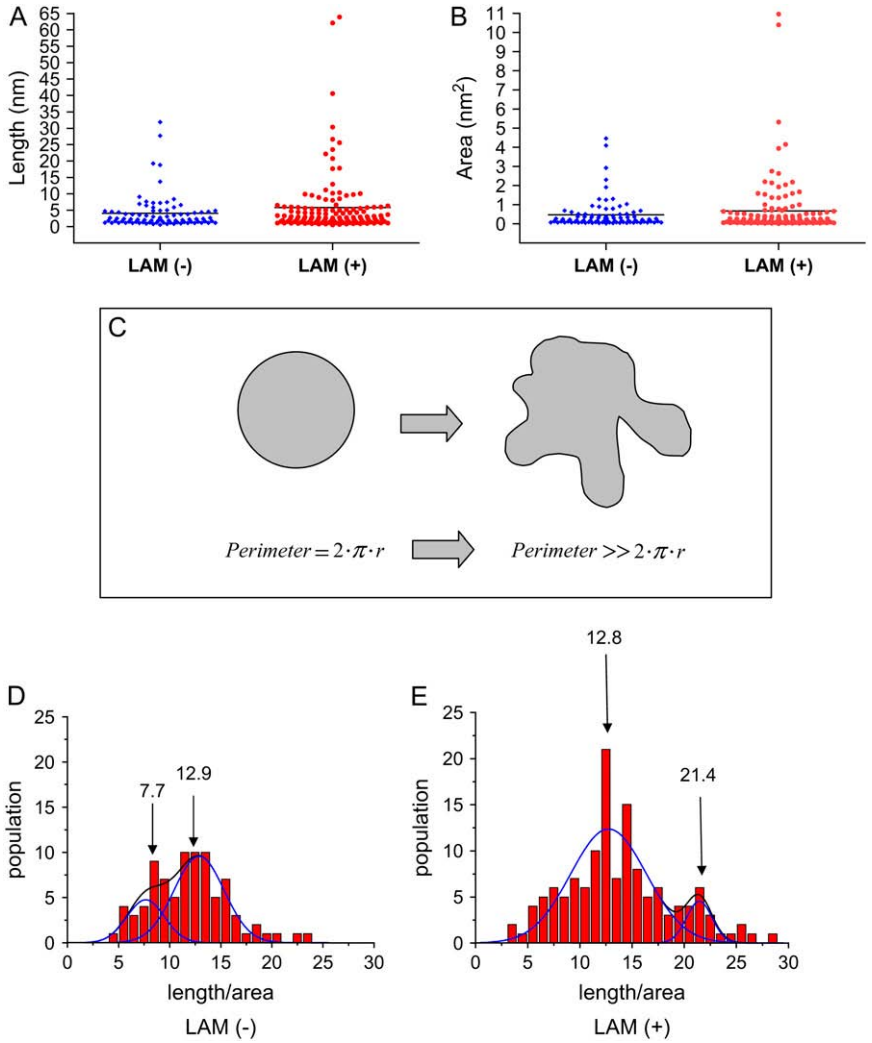

FIGURE 8 (*A* and *B*) Distributions of perimeter and area in LAM (−) and LAM (+) at 37°C. No significant difference between LAM (−) and LAM (+) in length and area was observed. (*C*) Concept for perimeter versus area size. When the object shape is a perfect circle, the area is $2\pi r$. However, if object shape becomes intricate, perimeter length becomes larger than a circle with the same area. At 37°C, in comparison to LAM-free vesicles (*D*), the shape and morphology of the SM-chol domains in a DOPC-SM-chol membrane were altered by the inclusion of LAM (*B*). SM-chol domains show two peaks in both LAM (−) and LAM (+) systems. However, at 37°C, the positions of LAM (+) peaks shifted to markedly higher values, implying that the shape of both populations of SM-chol domains have become increasingly more complex. An identical change was observed at 26°C, but not at 5°C (see Table 2).

may be restricted by the addition of LAM. Consequently, the miscibility of lipid molecules in the membrane would be relatively high, indicating a decrease in the importance of phase separations that result in more scattered and smaller SM-chol domains. The irregular domain structures revealed by AFM (cf. Fig. 5 *B*, Fig. 6, *D–F*) and the decreased sensitivity of domain shape to temperature variations support this hypothesis and provide critical insight into physical chemistry involved in LAM-induced inhibition of phospholipid fusion and the increased survival of MTB in humans.

These membrane domain modulations probably have an impact on the formation of intermediate structures such as ''stalks'' and/or ''pores'' after lipid mixing. The complex three-dimensional structure at the intermediate step may be altered by LAM molecules, resulting in a reduced total vesicle fusion as shown by FRET data.

TABLE 2 The effect of temperature and LAM on DOPC and SM-chol domain shape

	LAM −		LAM +	
Temp (°C)	Peak 1	Peak 2	Peak 1	Peak 2
5	8.4 ± 2.9	13.0 ± 4.4	10.2 ± 0.3	13.1 ± 0.7
26	10.2 ± 0.3	13.0 ± 0.5	17.2 ± 1.2	23.6 ± 2.5
37	7.7 ± 1.4	12.9 ± 0.9	12.8 ± 0.5	21.4 ± 0.7

Peak values obtained using multipeak Gaussian fitting of perimeter/area histograms are shown. At 5°C, LAM has minimal effect on the position of domain perimeter/area peaks in DOPC-SM-chol membranes. However, LAM induced marked increases in the complexity of domain shape at both 26°C and 37°C.

How does LAM inhibit P-L fusion in phagosome?

Based upon our cumulative data we can propose several pathways to explain the mechanism enabling the inhibition of P-L fusion by LAM. One possibility is that as a consequence of a LAM-induced modification of chol distribution due to the changes in membrane domain structure in the phagosomal membrane, TACO cannot surround and bind to the phagosomal membrane, resulting in reduced membrane associations. As we discussed above,

an anomalous state of membrane fusion may occur as a consequence of LAM-induced structural changes in the membrane.

The major difference between our in vitro vesicle fusion and P-L fusion in macrophages is the existence of the soluble *N*-ethylmaleimide-sensitive fusion attachment protein receptor (SNARE, (35)) complex instead of PEG. SNARE proteins and syntaxins 2, 3, and 4 are present on macrophages (36), making them potentially involved in the MTB-induced P-L fusion inhibition process. Based on our observations, it is possible that the function of SNARE proteins and their distribution are affected by LAM-induced domain modifications. Furthermore, it is also possible that SNARE complex members can be inhibited from interacting with each other or result in fewer interactions as a consequence of the large sugar moiety present on LAM, which is analogous to the reduction of the PEG effect in our in vitro system.

Lenz et al. (37) reported that SNAREs promote lipid membrane fusion in vitro but do not trigger membrane fusion. Logical extensions of their observation are 1), the inner membranes of fusing vesicles form intermediate structures at an early stage of the PEG-induced lipid vesicle fusion; 2), while intermediate structures are formed, local membrane curvature/surface lipid density and line tension are modulated by additional chol (38), resulting in the induction of vesicle fusion; and 3), if LAM is present in the system, LAM should induce an incommodity condition for the storks model membrane. As we found by AFM, SM-chol ''structural'' domains become irregularly scattered but more stable if LAM and chol are distributed in an irregular fashion in the membrane. As a result of stabilization, local regions of the membrane (e.g., the chol domain area) become three-dimensionally more rigid, resulting in the complete inhibition of vesicle fusion.

There is ample precedence for the premise presented here; some bacteria have been shown to modulate plasma membrane and (or) phagosomal membrane lipid rafts to facilitate their entry and survival in vertebrate cells (39,40). Therefore, both previous studies and our results support the possibility that MTB can escape the acidification process by a mechanism involving LAM-induced alterations in microdomain size and a concomitant decrease in the functionality of syntaxins in the liquid disorder phase. Recent studies demonstrate that sugar moieties and raft modifications are also involved in HIV-1 and influenza infections (41,42).

CONCLUSIONS

In this report, we elucidate that the physicochemical processes involved in LAM-induced modification of raft-like membrane structures correlate to an inhibition of lipid vesicle fusion. To our knowledge, this is the first demonstration that LAM changes the molecular packing efficiency of chol within the SM phase. The dramatic reorganization of the lipid membrane may be reflected in the inhibition of P-L fusion by MTB, survival of MTB within macrophages, and the onset of tuberculosis in humans. To understand details of inhibitory effects by LAM for the membrane fusion, further in vitro and in vivo systematic studies will be required using a variety of experimental conditions. Live cell imaging to study a direct correlation between domain modifications and inhibition of P-L fusions in vivo will be the most challenging work but provides a higher level of understanding. Another remaining question is what other factors may be involved in the inhibition of P-L fusion in macrophages. Long-chain sulfolipids also originate from MTB and may have similar effects. In summary, our findings strengthen the premise that an association exists between high glycolipid levels in MTBs and their ability to infect macrophages. In addition, it defines a possible role for glycolipid regulation in MTB survival. Absolute domain size differences may exist between in vitro versus in vivo systems, but these differences do not diminish the significance of our results, which may help in the development of unique new chemotherapeutics against MTB.

APPENDIX A

The normalized second-order intensity autocorrelation function determined by DLS in homodyne detection mode can be expressed as follows (Siegert relation):

$$g^{(2)}(\tau) = B + A|g^{(1)}(\tau)|^2, \tag{1}$$

where τ is the correlator delay time, B is the baseline value for the normalized correlation function measured at $\tau \rightarrow \infty$ and should be equal to 1 (subject to noise levels in the measured data), and A is an optical coherence factor that is instrument dependent but ideally equal to unity. The first-order electric field autocorrelation function, $g^1(\tau)$, is directly linked to the translational diffusion of the scatterers, and for independently diffusing polydisperse particles can be written in the form of a Laplace transform:

$$g^{(1)}(\tau) = \int_0^\infty G(\Gamma) \times \exp(-\Gamma\tau) d\Gamma, \tag{2}$$

where the decay rate $\Gamma = Dq^2$, D is the diffusion coefficient, $q = (4\pi n/\lambda_o)\sin(\theta/2)$ is the scattering vector, n is the refractive index of the medium, λ_o is the vacuum laser wavelength, and θ is the scattering angle. The function $G(\Gamma)$ describes the distribution of decay rates in the particle population and hence defines the particle size distribution.

The method of cumulants can be applied to extract information about the moments of the size distribution. Here the logarithm of $g^1(\tau)$ is expanded in a series to yield a polynomial in τ that can be analyzed by linear least squares fitting:

$$\ln[g^1(\tau)] = -K_1\tau + \frac{K_2}{2}\tau^2 \ldots \tag{3}$$

Only the first two terms are retained, whereas higher order terms are typically omitted. The first cumulant, $K_1 = \langle\Gamma\rangle$, yields the z-average particle size, and the dimensionless ratio, $K_2/\langle\Gamma\rangle^2$ (where K_2 is the second cumulant), defines a PI that characterizes the width of the distribution. For a Gaussian distribution of decay rates, $\sigma^2/2 = K_2 = PI \times \langle\Gamma\rangle^2$, where σ is the standard deviation of the distribution.

An inversion algorithm such as NNLS (23) can be used to deconvolute Eq. 2 and obtain an estimate of $G(\Gamma)$. NNLS seeks a nonnegative solution producing the best fit (minimum fit error) to the experimental data. By excluding solutions with physically unrealistic negative distribution values,

NNLS reduces the inherent ill-conditioned nature of Eq. 2, and thereby enables a larger number of possible solutions to be tested with the result that better size resolution is achieved. The algorithm yields a robust size distribution consistent with experimental data but without imposing the additional smoothness criteria required by regularization algorithms like CONTIN (43). Oversmoothing of the solution leads to a loss of size resolution, with the result that a real multimodal distribution might be represented after data inversion as a broad single peak.

APPENDIX B: SPHERICAL-SHELL MODEL OF LAM MOLECULES

The hydrodynamic radius of an arbitrary shaped body, RH, can be calculated following the classical theory of Bloomfield et al. (1967) from a representation of n spherical shells via the relationship

$$RH_{\mathrm{n}} = \frac{\left[\sum_{\mathrm{k}=0}^{\mathrm{n}} (R_{\mathrm{k}})^2\right]^2}{\left[\sum_{\mathrm{k}=0}^{\mathrm{n}} (R_{\mathrm{k}})^3\right] + 2\left[\sum_{\mathrm{i}2=1}^{\mathrm{n}} \sum_{\mathrm{i}1=0}^{\mathrm{i}2-1} \frac{(R_{\mathrm{i}2})^2 (R_{\mathrm{i}1})^2}{D_{\mathrm{i}2,\mathrm{i}1}}\right]}, \qquad (4)$$

where (44) R_{k} is the radius of the kth spherical shell and $D_{\mathrm{i}2,\mathrm{i}1}$ is the distance between the i2th and i1th spherical shells. The expression is considered to be exact within the Oseen-Burgers-Kirkwood formalism when the number n of the total spherical shell approaches infinity.

Our measurements of LAM vesicles are consistent with previous reports of the properties of LUVs extruded and maintained in a salt solution (26). Consequently, for a basic hydrodynamic model, we treat each LAM-free vesicle as one spherical shell of radius $RH_{\mathrm{V}} = 69.0$ nm (Fig. 2).

The molecular structure and hydrodynamics of LAM molecules are not known in great detail. Furthermore, their hydrodynamic structure when attached to or incorporated into a membrane can differ from their solution configuration. Therefore, we start from the basic assumption that each 17 KDa LAM molecule consists predominantly of 30 mannoses and 50 arabinofuranoses and both residues are ring-like water soluble units. The basic van der Waals dimension of the arabinofuranose unit is about 0.25 nm × 0.45 nm × 0.7 nm, the mannose unit is about 20% larger, and the bounded layer of water molecules is typically 0.3–0.5 nm.

Estimation of the hydrodynamic radius of a small molecule

The hydrodynamic radius of a small macromolecule can be estimated via the range, $[R_{\mathrm{sv}} \equiv \sqrt[3]{3V/4\pi} \le RH \le R_{\mathrm{SA}} \equiv \sqrt{(A/4\pi)}]$, where V is volume and A is the surface area of the molecule with its hydration layer, and the equalities hold for a spherical shape. Consequently, we can average over the two units and model each LAM molecule with 80 equal contacting spherical unit shells, each with a hydrodynamic radius, $Ru = 0.5$ nm, in a branched linear chain. Then, Eq. 4 can be applied to all specific conformations of such measured hydrodynamic properties. We numerically solved the case of a straight line of equal spherical shells and observed an empirical fit that

$$RH(n) \equiv C(n) \times Ru \cong [\sqrt{n} + 0.085 \times (n-2)] \times Ru; \quad 2 \le n \le 100. \qquad (5)$$

Therefore, for a LAM molecule configured into a small number of branches of tens of ring units, we have an acceptably robust estimation that $RH_{\mathrm{L}} \cong 13Ru \cong 6.5$ nm.

Spherical-shell model of LAM vesicles

Our DLS measurements on the LAM (+) vesicles are similar to those of LAM (−) vesicles except the mean hydrodynamic radius is increased to $RH_{\mathrm{VL}} = 75.3$ (Fig. 2). We presume that the underlying lipid vesicles are the same, and only LAM molecules externally attached to the lipid vesicles are responsible for the increase in the hydrodynamic radius. Eq. 4 can now be applied to spherical shells of unequal sizes to deduce the number of LAMs per vesicle. First for one LAM molecule as a spherical shell of $RH_{\mathrm{L}} \cong 6.5$ nm radius attached to the much larger spherical shell of radius $RH_{\mathrm{V}} \cong 69$ nm, Eq. 4 shows directly that the increment from one LAM molecule is $\delta RH_{\mathrm{L}} \cong 0.052$ nm. A linear extrapolation from the δRH_{L} value predicts that a total of $(\Delta RH_{\mathrm{L}}/\delta RH_{\mathrm{L}}) \cong 122$ LAM molecule shells attached to the outside of the membrane vesicle shell will account for the observed increase in the hydrodynamic radius. This linear extrapolation is independent of the relative locations of their representing spherical shells but does not yet account for any nonlinear multiple LAM shell effects. So as an improvement, we have considered a uniform placement of multiple LAM molecule shells outside of the vesicle shell and solved numerically that it takes $nL \cong 218$ LAM molecules to match the observed size increase, $\Delta RH_{\mathrm{L}} = RH_{\mathrm{LV}} - RH_{\mathrm{L}} \cong 6.3$ nm. The average distance between these LAM shells is $\sim\sqrt{4\pi/nL}(RH_{\mathrm{V}} + RH_{\mathrm{L}}) \cong 18$nm, so that LAM molecule shells are isolated from each other.

Therefore, we can conclude that about 218 LAM molecules are incorporated into the lipid bilayer with attachment to the outside of our LAM vesicles. LAM molecules attached to the inside of lipid vesicles do not affect hydrodynamic radius and are not directly measured by DSL. From the extrusion process, it is reasonable to expect a rough symmetry between the outside and inside leaflets of the lipid membrane. Consequently, we predict that there may be a total of about 436 LAM molecules incorporated into the underlying lipid LUV(s).

LAM/Lipid ratio in LAM vesicles

To estimate the LAM/lipid ratio, we now calculate the amount of lipids per LUV. Our LAM (−) and LAM (+) LUVs were extruded and maintained in a salt solution and were previously determined to have a certain degree elongation having the inverse of the elongation factor, p (i.e., the ratio of short axis b to the long axis a, with a prolate ellipsoid shape approximation) of ~3 (45). Following classical geometrical relations, we have deduced an explicit expression for membrane vesicle surface area as $A_{\mathrm{PE}}(RH, p) = 4\pi \times RH_{\mathrm{V}}^2 \times 2 \times S_{\mathrm{PE}}(p)$, where the extra factor of 2 accounts for the double leaflets of the bilayer and the shape function $S_{\mathrm{PE}}(p)$ depends on the vesicle elongation, p. Although our closed expression for $S_{\mathrm{PE}}(p)$ contains both Ln and $asin$ terms and is somewhat lengthy, it can be matched within 4% by a simple approximation, $S_{\mathrm{PE}}(p) \cong p^{-0.85}$ for $1 \le p^{-1} < 3.5$, such that $S_{\mathrm{PE}}(p) \cong 1$, 1.86, and 2.51 for $p^{-1} = 1$, 2, and 3, respectively. Thus, the lipid membrane surface area in our extruded LUV is about 2.5 times that of a sphere vesicle of radius RH.

Our membrane is composed of DOPC/SM/Chol in the ratio 5:5:3 (see Methods). Because of the complexity of the phase diagram, the mean surface area per lipid, A_{L}, is not exactly known, so we make the usual assumption that $A_{\mathrm{L}} \cong 0.7$ nm^2 per lipid weight of $MW_{\mathrm{DOPC}} \cong 800$ (45). Accordingly, we can calculate that the weight ratio of LAM to lipid in our LAM (+) LUV(s) is $\sim LL_{\mathrm{W}} \cong 2.2\%\{= 2 \times nL \times MW_{\mathrm{L}}/(4\pi RH_{\mathrm{L}}^2 \times 2.51 \times 2 \times MW_{\mathrm{DOPC}}/A_{\mathrm{L}})\}$. Considering that our initial sample contained LAM molecules of 1.8 wt % to DOPC/SM/Chol, one could conclude that most, if not all, LAM molecules are incorporated into LUV membranes.

SUPPLEMENTARY MATERIAL

To view all of the supplemental files associated with this article, visit www.biophysj.org.

We thank Dr. Kazuo Kobayashi, Department of Immunology, National Institute of Infectious Diseases, Japan, and Drs. Sohkichi Matsumoto and Nagatoshi Fujiwara, Graduate School of Medicine, Osaka City University, Japan, for discussions regarding MTB. Also we thank Drs. John F.

Andersen and Mihaela Crina Frincu, Laboratory of Malaria and Vector Research, National Institute of Allergy and Infectious Diseases, National Institutes of Health, for their critical readings of this manuscript. Certain trade names and company products are mentioned in the text or identified in illustrations to adequately specify the experimental procedure and equipment used. In no case does such an identification imply recommendation or endorsement by the National Institute of Standards and Technology, nor does it imply that the products are necessarily the best available for the purpose.

This work was supported in part by grants from the Precursory Research for Embryonic Science and Technology of the Japan Science and Technology Agency to E.H. and by the Intramural Research Program of the National Institute of Allergy and Infectious Diseases, National Institutes of Health.

REFERENCES

1. World Health Organization. 2005. WHO TB Epidemiology and Surveillance Virtual Workshop. http://www.who.int/tb/surveillance workshop/.
2. Beatty, W. L., E. R. Rhoades, H. J. Ullrich, D. Chatterjee, J. E. Heuser, and D. G. Russell. 2000. Trafficking and release of mycobacterial lipids from infected macrophages. *Traffic*. 1:235–247.
3. Doctors Without Borders. Tuberculosis. 2006. http://www.doctorswithoutborders.org/news/tuberculosis/index.cfm.
4. World Health Organization. 2003. Global and Regional Incidence. http://www.who.int/mediacentre/factsheets/fs104/en/.
5. Katalinic-Jankovic, V., and M. Obrovac. 2004. Drug-resistant tuberculosis: resistance mechanisms and drug susceptibility of Mycobacterium tuberculosis. *Acta Med. Croatica*. 58:323–328.
6. Brennan, P. J., and H. Nikaido. 1995. The envelope of mycobacteria. *Annu. Rev. Biochem.* 64:29–63.
7. Hunter, S. W., H. Gaylord, and P. J. Brennan. 1986. Structure and antigenicity of the phosphorylated lipopolysaccharide antigens from the leprosy and tubercle bacilli. *J. Biol. Chem.* 261:12345–12351.
8. Goren, M. B. 1970. Sulfolipid I of Mycobacterium tuberculosis, strain H37Rv. I. Purification and properties. *Biochim. Biophys. Acta*. 210:116–126.
9. Goren, M. B., P. D'Arcy Hart, M. R. Young, and J. A. Armstrong. 1976. Prevention of phagosome-lysosome fusion in cultured macrophages by sulfatides of Mycobacterium tuberculosis. *Proc. Natl. Acad. Sci. USA*. 73:2510–2514.
10. Fratti, R. A., J. Chua, I. Vergne, and V. Deretic. 2003. Mycobacterium tuberculosis glycosylated phosphatidylinositol causes phagosome maturation arrest. *Proc. Natl. Acad. Sci. USA*. 100:5437–5442.
11. Xu, S., A. Cooper, S. Sturgill-Koszycki, T. van Heyningen, D. Chatterjee, I. Orme, P. Allen, and D. G. Russell. 1994. Intracellular trafficking in Mycobacterium tuberculosis and Mycobacterium avium-infected macrophages. *J. Immunol.* 153:2568–2578.
12. Nigou, J., M. Gilleron, T. Brando, and G. Puzo. 2004. Structural analysis of mycobacterial lipoglycans. *Appl. Biochem. Biotechnol.* 118:253–267.
13. Kang, P. B., A. K. Azad, J. B. Torrelles, T. M. Kaufman, A. Beharka, E. Tibesar, L. E. Desjardin, and L. S. Schlesinger. 2005. The human macrophage mannose receptor directs Mycobacterium tuberculosis lipoarabinomannan-mediated phagosome biogenesis. *J. Exp. Med.* 202:987–999.
14. Vergne, I., J. Chua, and V. Deretic. 2003. Tuberculosis toxin blocking phagosome maturation inhibits a novel Ca2+/calmodulin-PI3K hVPS34 cascade. *J. Exp. Med.* 198:653–659.
15. Maiti, D., A. Bhattacharyya, and J. Basu. 2001. Lipoarabinomannan from Mycobacterium tuberculosis promotes macrophage survival by phosphorylating Bad through a phosphatidylinositol 3-kinase/Akt pathway. *J. Biol. Chem.* 276:329–333.
16. Pabst, M. J., J. M. Gross, J. P. Brozna, and M. B. Goren. 1988. Inhibition of macrophage priming by sulfatide from Mycobacterium tuberculosis. *J. Immunol.* 140:634–640.
17. Rousseau, C., O. C. Turner, E. Rush, Y. Bordat, T. D. Sirakova, P. E. Kolattukudy, S. Ritter, I. M. Orme, B. Gicquel, and M. Jackson. 2003. Sulfolipid deficiency does not affect the virulence of Mycobacterium tuberculosis H37Rv in mice and guinea pigs. *Infect. Immun.* 71:4684–4690.
18. Sahu, S., and W. S. Lynn. 1977. Lipid composition of human alveolar macrophages. *Inflammation*. 2:83–91.
19. Gatfield, J., and J. Pieters. 2000. Essential role for cholesterol in entry of mycobacteria into macrophages. *Science*. 288:1647–1650.
20. Ferrari, G., H. Langen, M. Naito, and J. Pieters. 1999. A coat protein on phagosomes involved in the intracellular survival of mycobacteria. *Cell*. 97:435–447.
21. Hamasur, B., G. Kallenius, and S. B. Svenson. 1999. A new rapid and simple method for large-scale purification of mycobacterial lipoarabinomannan. *FEMS Immunol. Med. Microbiol*. 24:11–17.
22. Pusey, P. N., and R. J. A. Tough. 1982. Dynamic light scattering, a probe of Brownian particle dynamics. *Adv. Colloid Interface Sci.* 16:143–159.
23. Morrison, I. D., E. F. Grabowski, and C. A. Herb. 1985. Improved techniques for particle size determination by quasi-elastic light scattering. *Langmuir*. 1:496–501.
24. Smolen, J. E. 2003. Liposomes in the study of membrane fusion in neutrophils. *Methods Enzymol.* 372: 300–319.
25. Malinin, V. S., M. E. Haque, and B. R. Lentz. 2001. The rate of lipid transfer during fusion depends on the structure of fluorescent lipid probes: a new chain-labeled lipid transfer probe pair. *Biochemistry*. 40:8292–8299.
26. Tokumasu, F., A. J. Jin, G. W. Feigenson, and J. A. Dvorak. 2003. Nanoscopic lipid domain dynamics revealed by atomic force microscopy. *Biophys. J.* 84:2609–2618.
27. Nettikadan, S., F. Tokumasu, and K. Takeyasu. 1996. Quantitative analysis of the transcription factor AP2 binding to DNA by atomic force microscopy. *Biochem. Biophys. Res. Commun.* 226:645–649.
28. Giocondi, M. C., S. Boichot, T. Plenat, and C. C. Le Grimellec. 2004. Structural diversity of sphingomyelin microdomains. *Ultramicroscopy*. 100:135–143.
29. Riviere, M., A. Moisand, A. Lopez, and G. Puzo. 2004. Highly ordered supra-molecular organization of the mycobacterial lipoarabinomannans in solution. Evidence of a relationship between supra-molecular organization and biological activity. *J. Mol. Biol.* 344:907–918.
30. Tokumasu, F., A. J. Jin, G. W. Feigenson, and J. A. Dvorak. 2003. Atomic force microscopy of nanometric liposome adsorption and nanoscopic membrane domain formation. *Ultramicroscopy*. 97:217–227.
31. van Duyl, B. Y., D. Ganchev, V. Chupin, B. de Kruijff, and J. A. Killian. 2003. Sphingomyelin is much more effective than saturated phosphatidylcholine in excluding unsaturated phosphatidylcholine from domains formed with cholesterol. *FEBS Lett.* 547:101–106.
32. Shabaana, A. K., K. Kulangara, I. Semac, Y. Parel, S. Ilangumaran, K. Dharmalingam, C. Chizzolini, and D. C. Hoessli. 2005. Mycobacterial lipoarabinomannans modulate cytokine production in human T helper cells by interfering with raft/microdomain signalling. *Cell. Mol. Life Sci.* 62:179–187.
33. Chernomordik, L. 1996. Non-bilayer lipids and biological fusion intermediates. *Chem. Phys. Lipids*. 81:203–213.
34. Hwang, J., L. K. Tamm, C. Böhm, T. S. Ramalingam, E. Betzig, and M. Edidin. 1995. Nanoscale complexity of phospholipid monolayers investigated by near-field scanning optical microscopy. *Science*. 270:610–614.
35. Weber, T., B. V. Zemelman, J. A. McNew, B. Westermann, M. Gmachl, F. Parlati, T. H. Sollner, and J. E. Rothman. 1998. SNAREpins: minimal machinery for membrane fusion. *Cell*. 92:759–772.

36. Hackam, D. J., O. D. Rotstein, M. K. Bennett, A. Klip, S. Grinstein, and M. F. Manolson. 1996. Characterization and subcellular localization of target membrane soluble NSF attachment protein receptors (t-SNAREs) in macrophages. Syntaxins 2, 3, and 4 are present on phagosomal membranes. *J. Immunol.* 156:4377–4383.

37. Dennison, S. M., M. E. Bowen, A. T. Brunger, and B. R. Lentz. 2006. Neuronal SNAREs do not trigger fusion between synthetic membranes but do promote PEG-mediated membrane fusion. *Biophys. J.* 90:1661–1675.

38. Kuzmin, P. I., S. A. Akimov, Y. A. Chizmadzhev, J. Zimmerberg, and F. S. Cohen. 2005. Line tension and interaction energies of membrane rafts calculated from lipid splay and tilt. *Biophys. J.* 88:1120–1133.

39. Norkin, L. C. 2001. Caveolae in the uptake and targeting of infectious agents and secreted toxins. *Adv. Drug Deliv. Rev.* 49:301–315.

40. Maldonado-Garcia, G., M. Chico-Ortiz, L. M. Lopez-Marin, and F. J. Sanchez-Garcia. 2004. High-polarity Mycobacterium avium-derived lipids interact with murine macrophage lipid rafts. *Scand. J. Immunol.* 60:463–470.

41. Fantini, J., D. Hammache, G. Pieroni, and N. Yahi. 2000. Role of glycosphingolipid microdomains in CD4-dependent HIV-1 fusion. *Glycoconj. J.* 17:199–204.

42. Shvartsman, D. E., M. Kotler, R. D. Tall, M. G. Roth, and Y. I. Henis. 2003. Differently anchored influenza hemagglutinin mutants display distinct interaction dynamics with mutual rafts. *J. Cell Biol.* 163:879–888.

43. Provencher, S. W. 1982. CONTIN: a general purpose constrained regularization program for inverting noisy linear algebraic and integral equations. *Comput. Phys. Commun.* 27:229–242.

44. Bloomfield, V., W. O. Dalton, and K. E. Van Holde. 1967. Frictional coefficients of multisubunit structures. I. Theory. *Biopolymers.* 5:135–148.

45. Jin, A. J., D. Huster, K. Gawrisch, and R. Nossal. 1999. Light scattering characterization of extruded lipid vesicles. *Eur. Biophys. J.* 28:187–199.